Electron-phonon interaction, lattice dynamics and superconductivity of an oxide spinel $LiTi_2O_4$

1994 J. Phys.: Condens. Matter 6 6997

(http://iopscience.iop.org/0953-8984/6/35/009)

J. Phys.: Condens. Matter 6 (1994) 6997–7012. Printed in the UK

Electron–phonon interaction, lattice dynamics and superconductivity of an oxide spinel $LiTi_2O_4$

Tatsuki Oda†, Masafumi Shirai†, Naoshi Suzuki† and Kazuko Motizuki‡§

† Department of Physics, Faculty of Engineering Science, Osaka University, Toyonaka 560, Japan

‡ Department of Physics, Faculty of Science, Sinshu University, Asahi 3–1–1, Matsumoto 390, Japan

Received 30 March 1994, in final form 24 May 1994

Abstract. The electron–phonon interaction of an oxide spinel $LiTi_2O_4$ is calculated on the basis of a realistic electronic band structure, which is obtained by the tight-binding model so as to reproduce the first-principles bands. The lattice dynamics of $LiTi_2O_4$ is studied by taking account of the effect of the electron–phonon interaction. Due to the characteristic dependences of the electron–phonon interaction on wavevectors and vibrational modes, a remarkable phonon frequency renormalization is found in the frequency range of 30–80 meV over a wide region of the Brillouin zone. By using the electron–phonon interaction and the renormalized phonon frequencies, the electron–phonon spectral function $\alpha^2F(\omega)$ is calculated to provide a basis for understanding the superconductivity of $LiTi_2O_4$. The superconducting transition temperature, gap functions, tunneling spectra and other thermodynamic properties are studied by solving the Eliashberg equation. The calculated results are in good agreement with observations.

1. Introduction

Among a large number of oxide spinels, only $LiTi_2O_4$ becomes a superconductor, with a transition temperature $T_c = 12\,K$ [1]. This value of T_c is notably higher than that of the other spinel-type superconductors, for example $CuRh_2S_4$ ($T_c = 3.5\,K$) and $CuRh_2Se_4$ ($T_c = 4.8\,K$) [2–4]. By substituting Li for Ti, $Li_{1+x}Ti_{2-x}O_4$ exhibits the metal–insulator transition at $x \simeq 0.1$ and becomes insulating for $0.1 \leqslant x \leqslant 1/3$ [1]. In the metallic phase ($x < 0.1$) T_c decreases monotonically with increasing x and vanishes at $x \simeq 0.1$.

$LiTi_2O_4$ has a normal spinel-type structure (space group $Fd3m$), in which Li and Ti atoms occupy the tetrahedral (8a) and octahedral (16d) sites, respectively. In the real structure O atoms are displaced from their ideal positions. The O displacements are described by a value of the internal structure parameter $u \simeq 0.26$. (Its ideal value is $u = 0.25$.) Due to the O displacements the octahedra around the Ti atoms exhibit trigonal distortion.

Recently, much effort has been made to clarify the mechanism of superconductivity in $LiTi_2O_4$ from both the experimental and the theoretical side, particularly in connection with the high-T_c copper-oxide superconductors. Judging from several experimental results, such as specific heat [5, 6] and tunneling spectra [7–9], it seems that the superconductivity of $LiTi_2O_4$ may be understood within the usual BCS-type mechanism.

§ Present address: Department of Physics, Faculty of Science, Okayama University of Science, Okayama 700, Japan.

0953-8984/94/356997+16$19.50

Electronic band structure calculations based on the local-density functional approximation have been performed for $LiTi_2O_4$ by Satpathy and Martin [10] with the use of the linear-muffin-tin orbital (LMTO) method and by Massidda and co-workers [11] with the use of the full-potential linearized augmented-plane-wave (FLAPW) method. Furthermore, Massidda and co-workers investigated the electron–phonon interaction on the basis of the rigid-muffin-tin approximation [12]. They estimated the dimensionless electron–phonon coupling constant λ and T_c by using the empirical McMillan formula [13]. However, their estimation of λ and T_c is insufficient because they related the averaged phonon frequency to the Debye frequency and dealt with it as a parameter.

The purposes of the present paper are, first, to clarify the role of the electron–phonon interaction in lattice dynamics and superconductivity of $LiTi_2O_4$ and, second, to study various superconducting properties in the framework of the usual phonon-mediated pairing mechanism. In section 2, the electron–phonon interaction is derived microscopically on the basis of the realistic tight-binding bands fitted to the first-principles bands [10, 11]. The lattice dynamics is studied by taking account of the effect of the electron–phonon interaction in section 3. In section 4, the electron–phonon spectral function $\alpha^2F(\omega)$ is calculated and T_c, gap functions, tunneling spectra and other thermodynamic properties are studied by solving the Eliashberg equation [14]. The results are compared with the observations and are discussed in connection with those obtained for $Ba_{1-x}K_xBiO_3$ and $La_{2-x}Sr_xCuO_4$ [15–19]. Finally, section 5 is devoted to a summary. Part of the present work has been reported elsewhere [20].

2. Electron–phonon interaction

According to the results of first-principles band calculations [10, 11], the Ti 3d conduction bands are separated by an energy gap of about 2.5 eV from the O 2p valence bands. The octahedral crystal-field splits the Ti 3d conduction bands into $3d\varepsilon$ and $3d\gamma$ bands, and the former are partially filled by one electron per formula unit. The overall features of the electronic density of states (DOS) for $LiTi_2O_4$ show good correspondence with the photoemission [21] and x-ray absorption [22] spectra.

The dispersion curves of the conduction bands crossing the Fermi level E_F in $LiTi_2O_4$ are well reproduced by the tight-binding model using the Slater–Koster transfer integrals for the neighbouring Ti–Ti, Ti–O and O–O pairs. The values of the Slater–Koster parameters used in the present calculation are listed in table 1. The calculated dispersion curves of the Ti $3d\varepsilon$ conduction bands near E_F are shown in figure 1. Two conduction bands ($n = 1, 2$) are partially filled by electrons for the real (distorted) structure.

The DOS at the Fermi level $N(E_F)$ is calculated as 3.0 states eV^{-1} per formula, which is comparable to the values obtained by first-principles band calculations, 3.3 [10] and 3.2 [11] states eV^{-1} per formula. The orbital components of the conduction band states at E_F are 82%, 11% and 7% for Ti $3d\varepsilon$, $3d\gamma$ and O 2p states, respectively. Thus, the conduction band states at E_F consist predominantly of the Ti $3d\varepsilon$ states. The hybridization between the Ti $3d\varepsilon$ and O 2p states is relatively weak and mainly caused by the transfer integral $t(dp\pi)_1$ for the nearest-neighbouring Ti–O pairs. Indeed, the first-principles band calculation has also shown that the conduction band states at E_F have about 9% contribution from O 2p states [11]. This nature of the conduction bands is in sharp contrast to the case of high-T_c cuprates, in which the conduction band states consist of the Cu $3d_{x^2-y^2}$ states hybridizing strongly with the O 2p states through $dp\sigma$ bonds.

The Fermi surfaces are composed of two pieces which have their necks toward the (111) direction in the Brillouin zone, as shown in figure 2. It is found that the Fermi

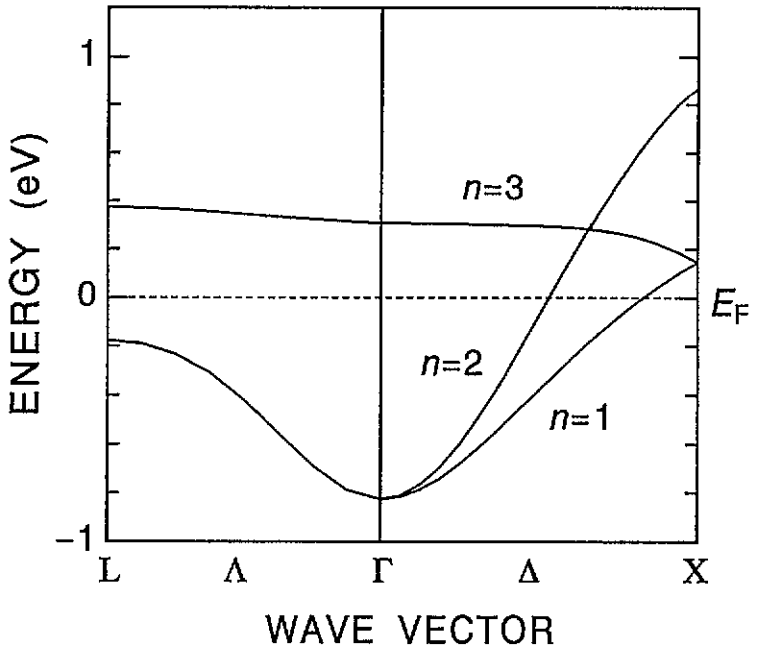

Figure 1. The dispersion curves of the Ti 3dε conduction bands near the Fermi level of $LiTi_2O_4$ calculated using the tight-binding model.

Table 1. The Slater–Koster transfer integrals and the orbital energies used in the tight-binding calculation.

	Distance (Å)	Transfer integral	Value (eV)
Ti–Ti	2.97	$t(\mathrm{dd}\sigma)$	−0.4070
		$t(\mathrm{dd}\pi)$	0.2400
		$t(\mathrm{dd}\delta)$	0.1500
Ti–O	2.00	$t(\mathrm{dp}\sigma)_1$	1.9700
		$t(\mathrm{dp}\pi)_1$	1.1850
	3.46	$t(\mathrm{dp}\sigma)_2$	−0.2450
		$t(\mathrm{dp}\pi)_2$	−0.1650
	3.71	$t(\mathrm{dp}\sigma)_3$	−0.2250
		$t(\mathrm{dp}\pi)_3$	−0.1630
O–O	2.67	$t(\mathrm{pp}\sigma)_1$	0.4725
		$t(\mathrm{pp}\pi)_1$	−0.0645
	2.98	$t(\mathrm{pp}\sigma)_2$	0.4525
		$t(\mathrm{pp}\pi)_2$	−0.0625
	3.27	$t(\mathrm{pp}\sigma)_3$	0.4325
		$t(\mathrm{pp}\pi)_3$	−0.0605
		Orbital energy	Value (eV)
Ti		$E(3\mathrm{d}\gamma)$	1.50
		$E(3\mathrm{d}\varepsilon)$	0.48
O		$E(2\mathrm{p})$	−4.95

surfaces of $LiTi_2O_4$ show no clear nesting features for particular wavevectors, unlike those of $Ba_{1-x}K_xBiO_3$ and $La_{2-x}Sr_xCuO_4$ [15–19].

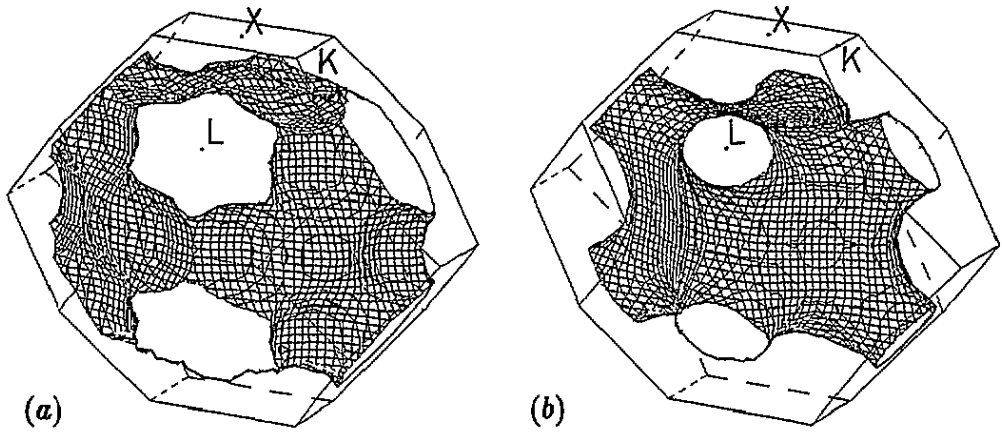

Figure 2. The Fermi surfaces of (*a*) the lower ($n = 1$) and (*b*) the upper ($n = 2$) conduction bands of $LiTi_2O_4$ calculated by the tight-binding model.

In the tight-binding approximation the electron–phonon coupling arises from modulation of the transfer integrals due to atomic displacements [23]. The electron–phonon coupling coefficient is given by

$$V^{\gamma}(n\boldsymbol{k}, n'\boldsymbol{k}-\boldsymbol{q}) = \sum_{\mu\alpha} \frac{1}{\sqrt{M_\mu}} \varepsilon_{\gamma,\mu\alpha}(\boldsymbol{q}) g^{\alpha}_{\mu}(n\boldsymbol{k}, n'\boldsymbol{k}-\boldsymbol{q}) \tag{1}$$

where γ specifies the phonon mode, $\varepsilon_{\gamma,\mu\alpha}(\boldsymbol{q})$ denotes the phonon polarization vector and M_μ is the mass of the μth atom. The coupling coefficient $g^{\alpha}_{\mu}(n\boldsymbol{k}, n'\boldsymbol{k}-\boldsymbol{q})$ between two conduction band states $n\boldsymbol{k}$ and $n'\boldsymbol{k}-\boldsymbol{q}$ caused by displacement of the μth atom in the unit cell along the α direction ($\alpha = x, y, z$) is expressed as

$$g^{\alpha}_{\mu}(n\boldsymbol{k}, n'\boldsymbol{k}-\boldsymbol{q}) = \sum_{\mu' a} \sum_{\nu' b} [A^{\dagger}(\boldsymbol{k})]_{n,\mu' a} [\dot{T}^{\alpha}_{\mu}(\boldsymbol{k}, \boldsymbol{k}-\boldsymbol{q})]_{\mu' a,\nu' b} [A(\boldsymbol{k}-\boldsymbol{q})]_{\nu' b,n'} \tag{2}$$

where $A(\boldsymbol{k})$ denotes the transformation matrix that diagonalizes the Hamiltonian matrix of the original structure, and $\dot{T}^{\alpha}_{\mu}(\boldsymbol{k}, \boldsymbol{k}-\boldsymbol{q})$ is expressed in terms of derivatives of the transfer integrals.

For the derivatives of the transfer integrals we consider only $t'(\mathrm{dp}\pi)_1$ for the nearest-neighbouring Ti–O pairs and $t'(\mathrm{dd}\sigma)$, $t'(\mathrm{dd}\pi)$, $t'(\mathrm{dd}\delta)$ for the neighbouring Ti–Ti pairs, since the conduction band states around E_F consist mainly of Ti $3d\varepsilon$ states. In the present paper the following values are used: $t'(\mathrm{dp}\pi)_1 = -7.0$, $t'(\mathrm{dd}\sigma) = 0.39$, $t'(\mathrm{dd}\pi) = -0.23$, $t'(\mathrm{dd}\delta) = -0.14$ in $\mathrm{eV\,\AA^{-1}}$. These parameter values are deduced from the following procedure. According to the FLAPW band calculations for $LiTi_2O_4$ [11], the energy bands having the Γ_1 symmetry at $\boldsymbol{k} = 0$ are most affected by the change of the structural parameter u. We have estimated the values of $t(\mathrm{dp}\pi)_1$ for both the real ($u = 0.2626$) and the ideal ($u = 0.25$) structures, so as to reproduce the energy eigenvalues with the Γ_1 symmetry. As the result, we obtain $t(\mathrm{dp}\pi)_1 = 1.19 \pm 0.09\,\mathrm{eV}$ and $0.60 \pm 0.04\,\mathrm{eV}$ for the real and the ideal structures, respectively. By assuming a linear dependence of $t(\mathrm{dp}\pi)_1$ on the nearest-neighbouring Ti–O bond length $d_{\mathrm{Ti-O}}$, the gradient $t'(\mathrm{dp}\pi)_1$ is evaluated to be $-5.9 \pm 1.3\,\mathrm{eV\,\AA^{-1}}$ since $d_{\mathrm{Ti-O}}$ is 2.00 Å and 2.10 Å for the real and the ideal structures, respectively. In the present paper we adopt a value, $-7.0\,\mathrm{eV\,\AA^{-1}}$, which is an upper bound

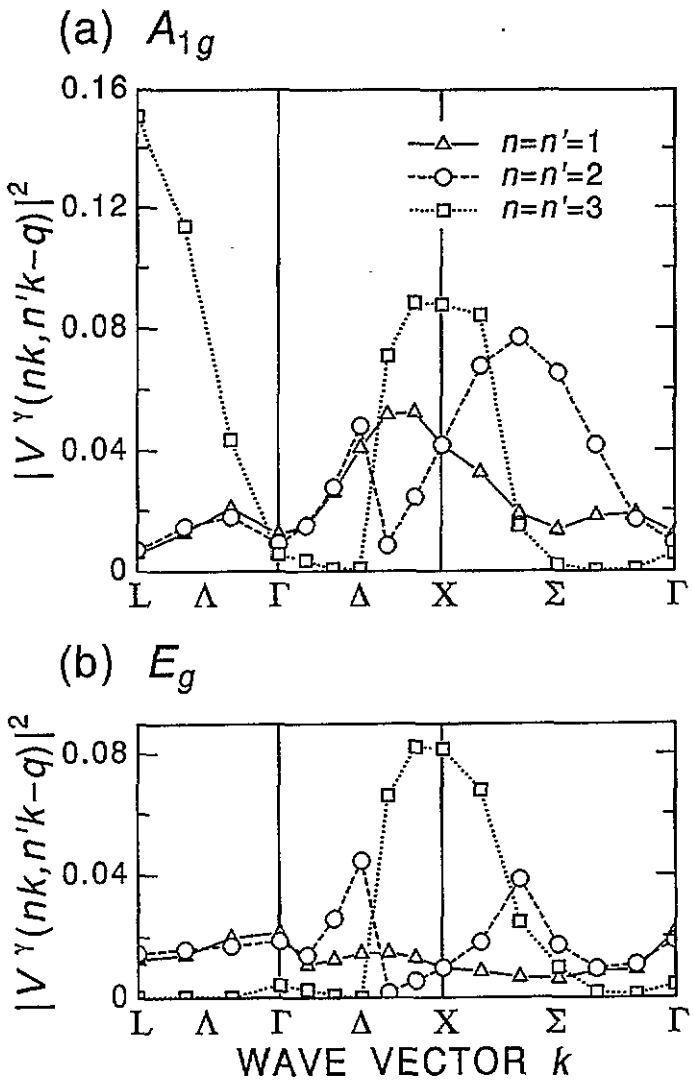

Figure 3. The electron–phonon coupling coefficient $|V^{\gamma}(nk, n'k-q)|^2$ of $LiTi_2O_4$ as a function of wavevector k for (*a*) the A_{1g} and (*b*) the E_g phonon modes at the Γ point ($q = 0$). Only the intraband coupling for the lowest three Ti 3*d*σ conduction bands ($n = n' = 1, 2, 3$) are shown.

of the above estimation. The ratio of $t'(\mathrm{dd}\sigma) : t'(\mathrm{dd}\pi) : t'(\mathrm{dd}\delta)$ is assumed to be equal to that of $t(\mathrm{dd}\sigma) : t(\mathrm{dd}\pi) : t(\mathrm{dd}\delta)$. Then, the ratio of $t'(\mathrm{dp}\pi)_1 : t'(\mathrm{dd}\sigma)$ is determined so as to reproduce the ratio of the McMillan–Hopfield parameters, $\eta_{\mathrm{Ti}} : \eta_{\mathrm{O}}$, obtained by the rigid-muffin-tin approximation [11].

In figures 3(*a*) and (*b*), for instance, the intraband ($n = n'$) electron–phonon coupling coefficient $|V^{\gamma}(nk, n'k-q)|^2$ is shown as a function of wavevector k for the A_{1g} and the E_g phonon modes at the Γ point ($q = 0$), respectively. Both phonon modes are composed of the vibrations of O atoms. The interband electron–phonon coupling is weaker than the intraband electron–phonon coupling for these phonon modes. It is found that the electron–phonon coupling shows remarkable dependences on wavevectors and phonon modes. It is

noted that the electron–phonon coupling for the A_{1g} and the E_g phonon modes is particularly stronger than that for the other modes at the Γ point, as shown later.

3. Lattice dynamics

The lattice dynamics of $LiTi_2O_4$ has been studied by taking account of effective long-range interatomic forces caused by the electron–phonon interaction. The Fourier transform of the effective long-range interatomic forces, i.e. the generalized electronic susceptibility, is expressed as

$$\chi^{\alpha\beta}_{\mu\nu}(q) = -2\sum_{nn'}\sum_{k} g^{\alpha}_{\mu}(nk, n'k-q)g^{\beta}_{\nu}(nk, n'k-q)^{*}\frac{f(E^0_{nk}) - f(E^0_{n'k-q})}{E^0_{n'k-q} - E^0_{nk}} \tag{3}$$

where $g^{\alpha}_{\mu}(nk, n'k-q)$ is the electron–phonon coupling coefficient defined by (2), E^0_k denotes the conduction band energy in the original structure and $f(E^0_k)$ is the Fermi distribution function.

For short-range interatomic forces we have considered six kinds of stretching-type forces for Li–O, Ti–O, Ti–Ti and O–O neighbouring pairs. These force constants are determined by referring to the force constants for other oxide spinels [24, 25], since no sufficient data for phonons of $LiTi_2O_4$ are available so far. The force constants used in the present paper are listed in table 2.

Table 2. The stretching-type short-range interatomic force constants used in the lattice dynamical calculation.

	Distance (Å)	Force constant (10^5 dyn cm^{-1})
Li–O	2.00	1.0
Ti–O	2.00	1.0
Ti–Ti	2.97	0.8
O–O	2.67	0.2
	2.98	0.2
	3.27	0.2

The phonon dispersion curves calculated along the (100), (110) and (111) directions are shown in figure 4(*a*). In this figure full curves represent the phonon dispersion curves calculated by including the effect of the electron–phonon interaction, i.e. $\chi(q)$, and broken curves represent those calculated with neglect of $\chi(q)$. Frequency renormalization due to the electron–phonon interaction is found in the frequency range of 30–80 meV over a wide region of the Brillouin zone. This fact is in sharp contrast to the frequency renormalization obtained for $Ba_{1-x}K_xBiO_3$ and $La_{2-x}Sr_xCuO_4$, in which a remarkable frequency renormalization occurs around specific positions in the Brillouin zone [15–19]. The difference in the wavevector dependence of the phonon frequency renormalization between $LiTi_2O_4$ and $Ba_{1-x}K_xBiO_3$ (or $La_{2-x}Sr_xCuO_4$) is primarily due to the absence of the Fermi surface nesting in $LiTi_2O_4$.

The phonon density of states (PDOS) including the effect of the electron–phonon interaction is shown in figure 4(*b*). Below 80 meV, vibrations of Ti and O atoms hybridize well with each other, while vibrations of Li atoms mainly appear near 85 meV. In the

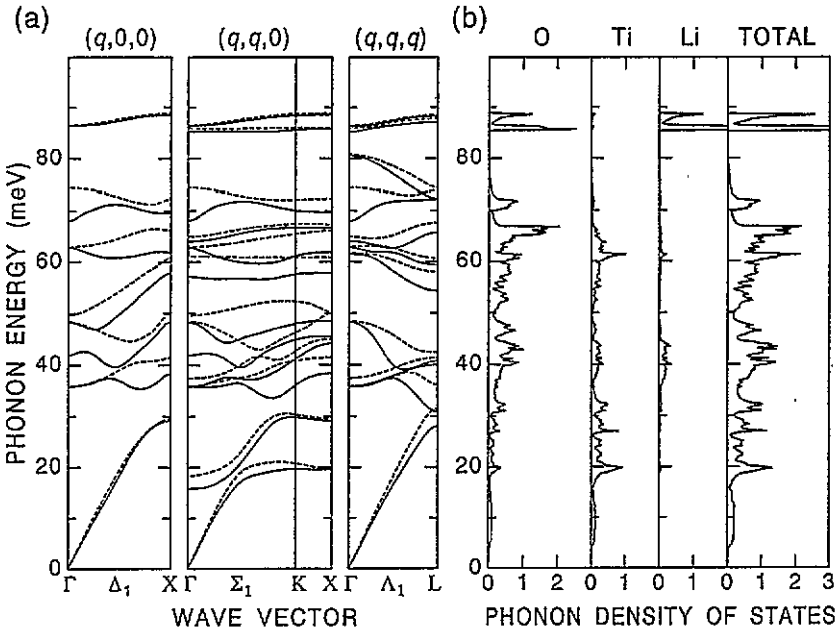

Figure 4. (*a*) The phonon dispersion curves of $LiTi_2O_4$ having the Δ_1, Σ_1, and Λ_1 symmetries along the (100), (110) and (111) directions, respectively, including (full curves) and without (broken curves) the effect of the electron–phonon interaction. (*b*) The phonon density of states (PDOS) of $LiTi_2O_4$ including the effect of the electron–phonon interaction. The PDOS projected to the vibrational components of each constituent atom of $LiTi_2O_4$ is also shown. The unit of the PDOS is meV^{-1} per unit cell.

frequency range 30–80 meV, where phonon frequencies are renormalized notably and thus phonons couple strongly with conduction electrons, the vibrations of O atoms as well as those of Ti atoms are primarily involved. Available experimental data about the phonons in $Li_{1+x}Ti_{2-x}O_4$ are only the PDOS observed by inelastic neutron scattering using time-of-flight method for both $LiTi_2O_4$ and insulating $Li_{4/3}Ti_{5/3}O_4$ [26]. According to the experimental results a pronounced change of the PDOS has been observed in the frequency range 40–70 meV, going from $Li_{4/3}Ti_{5/3}O_4$ to $LiTi_2O_4$. This observation may be regarded as experimental evidence for the phonon renormalization due to the electron–phonon interaction. More experimental information, for example Raman scattering or infrared absorption, is highly desired for further comparison.

The phonon linewidth caused by the electron–phonon interaction is calculated by using the expression [27]

$$\Gamma_{q\gamma} = \pi \sum_{nn'} \sum_{k} |V^{\gamma}(nk, n'k-q)|^2 \delta(E^0_{nk} - E_F)\delta(E^0_{n'k-q} - E_F) \qquad (4)$$

where $V^{\gamma}(nk, n'k-q)$ is the electron–phonon coupling coefficient defined by (1). The calculated phonon linewidth, together with the bare and renormalized phonon frequencies, for each phonon mode at the Γ and X points, are listed in tables 3 and 4, respectively. At the Γ point the phonon linewidth is particularly broad for the A_{1g} and the E_g modes, whose renormalized frequencies are 68.00 and 41.83 meV, respectively. On the other hand, at the X point several phonon modes, whose renormalized frequencies are in the range 40–70 meV,

have a relatively broad linewidth compared with the other phonon modes. However, their values of the phonon linewidth are an order of magnitude smaller than those of the A_{1g} and the E_g modes at the Γ point.

Table 3. The bare and renormalized phonon frequencies, linewidth and dimensionless coupling constant $\lambda_{q\gamma}$ for each phonon mode at the Γ point $q = (0, 0, 0)$.

	Frequency (meV)		Linewidth (meV)	$\lambda_{q\gamma}$
	Bare	Renormalized		
A_{1g}	74.45	68.00	5.734	0.151
A_{2u}	80.84	80.65	0.	0.
	61.76	61.53	0.	0.
T_{1g}	49.46	49.33	0.039	0.002
T_{1u}	86.48	86.39	0.	0.
	63.00	62.83	0.	0.
	48.48	48.29	0.	0.
	35.91	35.86	0.	0.
	0.	0.	—	—
T_{2g}	85.88	85.27	0.323	0.005
	66.08	64.07	0.460	0.014
	37.42	35.80	0.390	0.037
T_{2u}	61.12	57.19	0.051	0.002
	18.41	15.93	0.012	0.006
E_g	49.58	41.83	2.844	0.198
E_u	70.42	70.10	0.023	0.001
	35.81	35.53	0.008	0.001

4. Superconductivity

4.1. Electron–phonon spectral function

In order to study the superconductivity of $LiTi_2O_4$ in the framework of the usual phonon-mediated pairing mechanism, we have calculated the electron–phonon spectral function defined by [27, 28]

$$\alpha^2F(\omega) = \frac{1}{N(E_F)}\sum_{nn'}\sum_{k}\sum_{q\gamma}\frac{|V^{\gamma}(nk, n'k-q)|^2}{2N\omega_{q\gamma}}\delta(E^0_{nk} - E_F)\delta(E^0_{n'k-q} - E_F)\delta(\omega - \omega_{q\gamma})$$
$$= \frac{1}{2\pi NN(E_F)}\sum_{q\gamma}\frac{\Gamma_{q\gamma}}{\omega_{q\gamma}}\delta(\omega - \omega_{q\gamma}) \tag{5}$$

where $\omega_{q\gamma}$ and $\Gamma_{q\gamma}$ denote the renormalized phonon frequency and the linewidth having wavevector q and mode γ, respectively.

In figure 5, the calculated $\alpha^2F(\omega)$ is shown together with the total PDOS for comparison. The shape of $\alpha^2F(\omega)$ differs from that of the PDOS. The spectral function $\alpha^2F(\omega)$ takes large values in the frequency range 30–80 meV, where the vibrations of O atoms are mainly involved and hybridize with those of Ti atoms. Therefore, the vibrations of O atoms as well as of Ti atoms in this wide frequency range contribute to the superconductivity of $LiTi_2O_4$.

Table 4. The bare and renormalized phonon frequencies, linewidth and dimensionless coupling constant $\lambda_{q\gamma}$ for each phonon mode at the X point $q = (2\pi/a, 0, 0)$.

	Frequency (meV)		Linewidth (meV)	$\lambda_{q\gamma}$
	Bare	Renormalized		
X_1	88.91	88.57	0.097	0.002
	72.32	69.64	0.323	0.008
	66.17	61.91	0.584	0.019
	60.88	57.88	0.417	0.015
	50.26	48.50	0.214	0.011
	41.43	38.34	0.456	0.038
	29.61	29.13	0.058	0.008
X_2	65.92	64.18	0.109	0.003
	49.53	46.35	0.464	0.026
	28.51	27.33	0.023	0.004
X_3	85.99	85.60	0.058	0.001
	64.81	64.01	0.019	0.001
	60.54	59.28	0.023	0.001
	38.20	36.84	0.109	0.010
	28.90	28.51	0.008	0.001
	13.94	12.77	0.012	0.009
X_4	86.04	85.82	0.051	0.001
	67.31	66.69	0.113	0.003
	50.07	45.50	0.880	0.052
	45.05	44.17	0.238	0.015
	19.69	19.53	0.004	0.001

By using $\alpha^2F(\omega)$ shown in figure 5, the dimensionless electron–phonon coupling constant defined by

$$\lambda = 2\int_0^\infty \frac{d\omega}{\omega}\alpha^2F(\omega) \tag{6}$$

is evaluated to be 0.657, which is comparable to that obtained by Massidda and co-workers on the basis of the rigid-muffin-tin approximation [11]. The dimensionless coupling constant λ can be decomposed into the contribution from each phonon mode as follows:

$$\lambda = \frac{1}{N}\sum_{q\gamma}\lambda_{q\gamma} \tag{7}$$

where

$$\lambda_{q\gamma} = \frac{1}{\pi N(E_F)}\frac{\Gamma_{q\gamma}}{\omega_{q\gamma}^2}. \tag{8}$$

The values of $\lambda_{q\gamma}$ calculated for the phonon modes at the Γ and X points are listed in tables 3 and 4, respectively. It is found that the A_{1g} and the E_g modes contribute predominantly to λ at the Γ point, whereas several phonon modes in the range 40–70 meV contribute to λ at the X point.

The logarithmically averaged phonon frequency defined by

$$\langle\omega\rangle_{ln} = \exp\left(\frac{2}{\lambda}\int_0^\infty \frac{d\omega}{\omega}\alpha^2F(\omega)\ln\omega\right) \tag{9}$$

is evaluated to be 28.2 meV, which is relatively small compared with that obtained for $Ba_{1-x}K_xBiO_3$ ($\langle\omega\rangle_{ln} = 42$ meV) [15, 16].

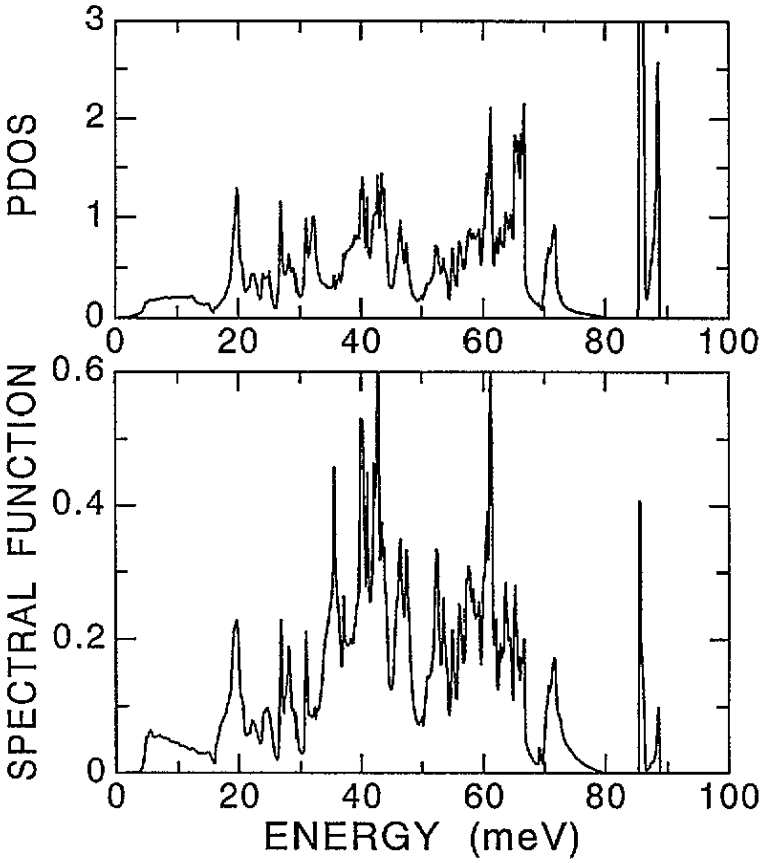

Figure 5. The electron–phonon spectral function $\alpha^2F(\omega)$ of $LiTi_2O_4$ (the lower panel). The total phonon density of states (PDOS) is also shown for comparison (the upper panel).

4.2. *Superconducting properties*

On the basis of $\alpha^2F(\omega)$ obtained above, various superconducting properties are studied by solving the Eliashberg equation at finite temperatures [14, 29, 30]:

$$\Delta(\mathrm{i}\omega_n) = \frac{\pi k_B T}{Z(\mathrm{i}\omega_n)} \sum_m \frac{\Delta(\mathrm{i}\omega_m)}{\sqrt{\omega_m^2 + \Delta^2(\mathrm{i}\omega_m)}} [\lambda(\mathrm{i}\omega_m - \mathrm{i}\omega_n) - \mu^* \theta(\omega_c - |\omega_m|)] \tag{10}$$

$$Z(\mathrm{i}\omega_n) = 1 + \frac{\pi k_B T}{\omega_n} \sum_m \frac{\omega_m}{\sqrt{\omega_m^2 + \Delta^2(\mathrm{i}\omega_m)}} \lambda(\mathrm{i}\omega_m - \mathrm{i}\omega_n) \tag{11}$$

where $\Delta(\mathrm{i}\omega_n)$ and $Z(\mathrm{i}\omega_n)$ denote the gap function and the renormalization function, respectively, defined at the Matsubara imaginary frequency $\mathrm{i}\omega_n = (2n+1)\mathrm{i}\pi k_B T$ with n an integer

$$\lambda(\mathrm{i}\omega_m - \mathrm{i}\omega_n) = 2 \int_0^\infty \alpha^2 F(\Omega) \frac{\Omega}{\Omega^2 + (\omega_n - \omega_m)^2} \mathrm{d}\Omega \tag{12}$$

and μ^* represents the screened Coulomb repulsion constant which is to be used with a cutoff frequency ω_c. In the present paper we adopt $\mu^* = 0.1$ and $\omega_c = 500\,\mathrm{meV}$.

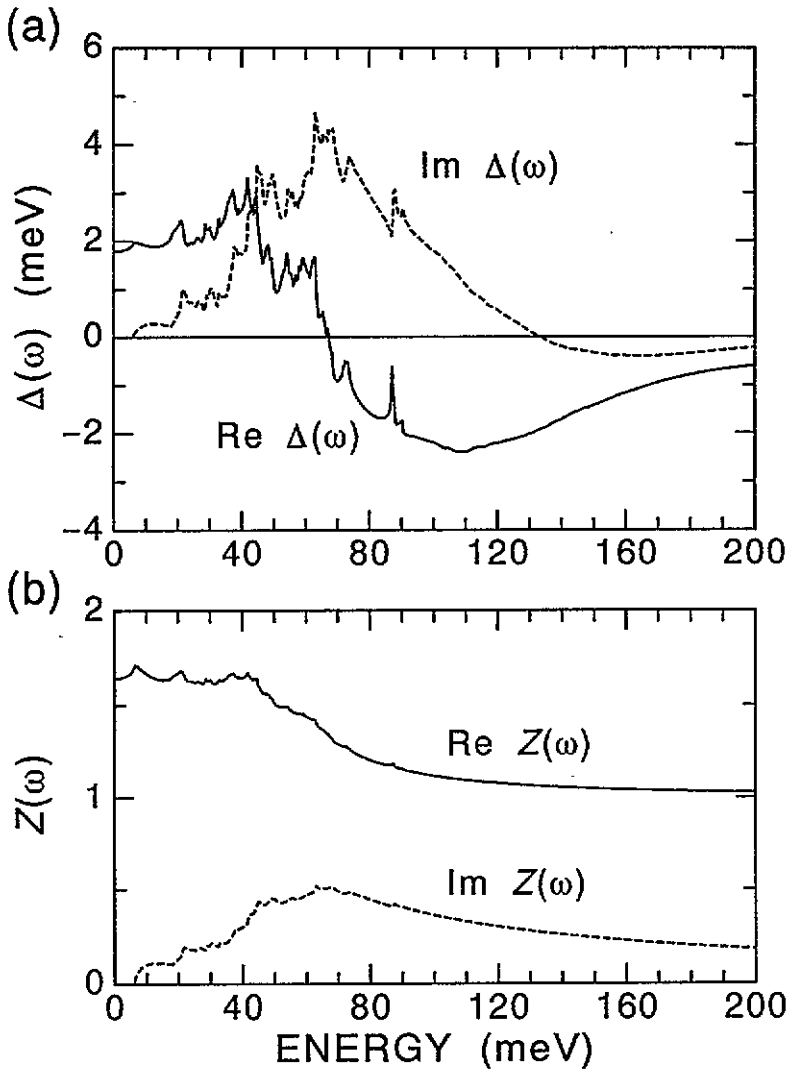

Figure 6. (*a*) The gap function $\Delta(\omega)$ and (*b*) the renormalization function $Z(\omega)$ of $LiTi_2O_4$ calculated at $T = 0.1T_c$. The full (broken) curves represent the real (imaginary) part.

First, in order to obtain T_c, we solved the Eliashberg equation linearized with respect to the gap function $\Delta(i\omega_n)$ [31]. The value of T_c is evaluated to be 10.9 K, which agrees well with the experimental values as listed in table 5.

On the other hand, in order to obtain the superconducting gap edge Δ_0 below T_c, we calculated the gap function $\Delta(\omega)$ and the renormalization function $Z(\omega)$ defined at real frequencies by using a method for the analytic continuation developed by Marsiglio and co-workers [32]. In figures 6(*a*) and (*b*) $\Delta(\omega)$ and $Z(\omega)$ calculated at $T = 0.1T_c$ are shown, respectively. It is found that $\Delta(\omega)$ has sharp and prominent peaks below 90 meV, reflecting the peaks in $\alpha^2F(\omega)$ (see also figure 5).

At $T = 0.1T_c$ (= 1.09 K) the gap edge Δ_0, defined by $\Delta_0 = \mathrm{Re}\Delta(\Delta_0)$, is evaluated to be 1.79 meV. As listed in table 5, this theoretical value is in good agreement with the

Table 5. The theoretical and experimental values of the superconducting transition temperature T_c, the gap edge Δ_0, their ratio $2\Delta_0/k_BT_c$ and the normalized specific heat discontinuity at T_c, $\Delta C/\gamma T_c$ (γ is the Sommerfeld constant), of $LiTi_2O_4$.

	T_c (K)	Δ_0 (meV)	$2\Delta_0/k_BT_c$	$\Delta C/\gamma T_c$
Theory				
Present work	10.9	1.79	3.84	1.70
Tunneling experiments				
Ref. [8]	11.3	1.95 ± 0.03	4.00±0.06	—
Ref. [9]	11.5	1.80 ± 0.05	3.55±0.15	—
Specific heat experiments				
Ref. [6]	12.4	2.03	3.8	1.57
Ref. [5]	11.7	—	—	1.59

experimental values obtained by tunneling measurements at 4.2 K [8,9] and specific heat measurements at low temperatures [6]. In the present calculation the ratio $2\Delta_0/k_BT_c$ is evaluated to be 3.84, which is slightly larger than the value 3.53 predicted in the BCS weak-coupling theory [33]. In figure 7, Δ_0 is shown as a function of temperature. The temperature dependence of Δ_0 calculated for $LiTi_2O_4$ is quite similar to that predicted in BCS theory [33]. Indeed, it has been confirmed by tunneling measurements [9] that the temperature dependence of Δ_0 is consistent with the BCS prediction.

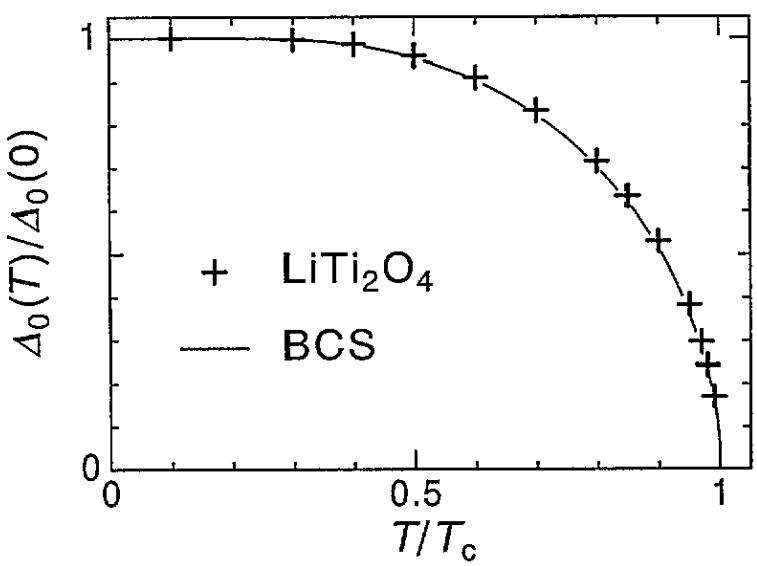

Figure 7. The temperature dependence of the superconducting gap edge Δ_0 calculated for $LiTi_2O_4$ (crosses). That obtained from the BCS theory [33] is also shown (full curve).

Tunneling spectra have been calculated with the use of $\Delta(\omega)$ obtained at $T = 0.1T_c$. The calculated differential conductance dI/dV and its derivative d^2I/dV^2 are shown by the full curves in figures 8(*a*) and (*b*), respectively. These curves show prominent structures, which reflect the peak structures in $\alpha^2F(\omega)$, and deviate from the BCS results [33] shown by the broken curves. Such deviations have not been observed in tunneling measurements

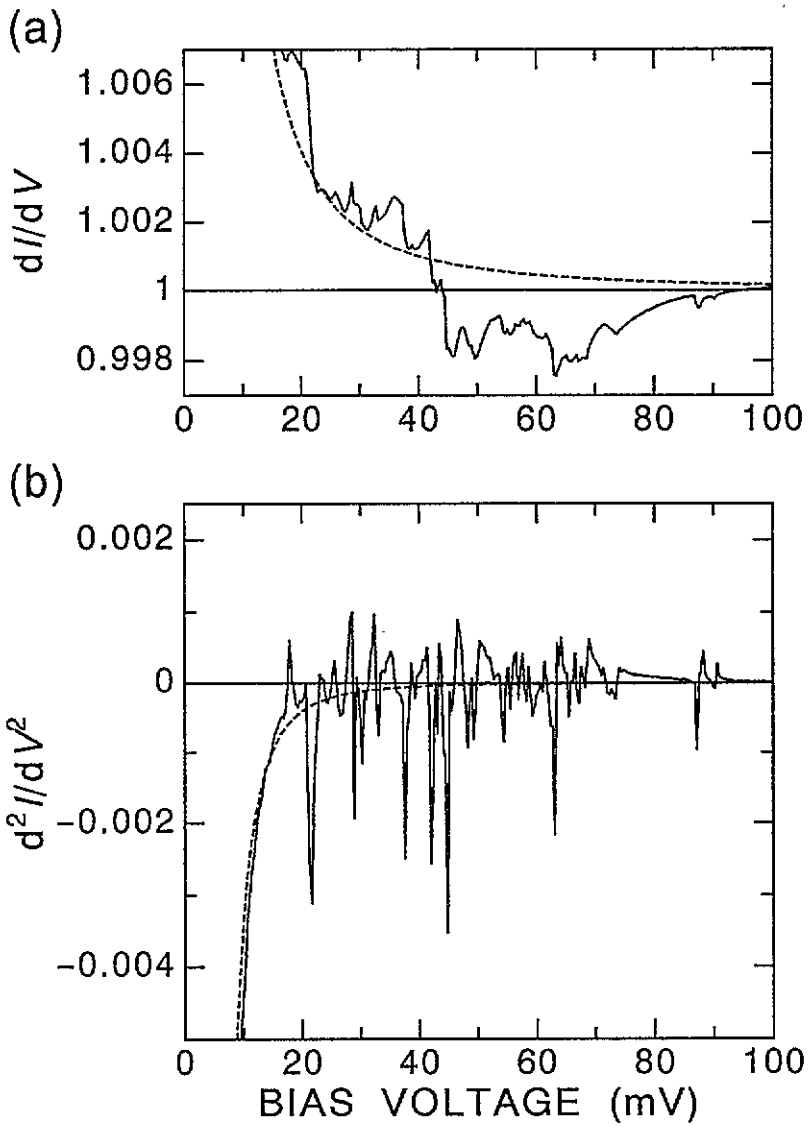

Figure 8. (*a*) The tunneling conductance dI/dV and (*b*) its derivative d^2I/dV^2 of $LiTi_2O_4$ calculated with the use of the gap function obtained by solving the Eliashberg equation at $T = 0.1T_c$ (full curves). Those obtained from the BCS theory [33] are also shown (broken curves).

yet. Since the deviations are an order of magnitude smaller than those obtained previously for $Ba_{1-x}K_xBiO_3$ and $La_{2-x}Sr_xCuO_4$ [15–19], more precise tunneling measurements are necessary to detect the fine structures predicted in the present calculation.

The thermodynamic critical field $H_c(T)$ can be calculated by using the solution of the Eliashberg equation, $\Delta(i\omega_n)$ and $Z(i\omega_n)$ [29, 34, 35]. In figure 9 the deviation of the reduced critical field $H_c(T)/H_c(0)$ from a parabolic curve $[1 - (T/T_c)^2]$ is shown as a function of the square of the reduced temperature $(T/T_c)^2$. For comparison, the critical field deviation for Pb is also calculated with the use of $\alpha^2F(\omega)$ deduced from the tunneling spectra by

McMillan and Rowell [36]. The present result for Pb is essentially the same as that obtained by Swihart and co-workers [37] based on a model of $\alpha^2F(\omega)$. The critical field deviation for $LiTi_2O_4$ is clearly different from that obtained from the BCS weak-coupling theory [33]. However, the critical field deviation for $LiTi_2O_4$ is still negative at all temperatures below T_c, unlike that for a typical strong-coupling superconductor Pb. Therefore, it is suggested that $LiTi_2O_4$ is a superconductor that has a phonon-mediated pairing interaction of intermediate strength.

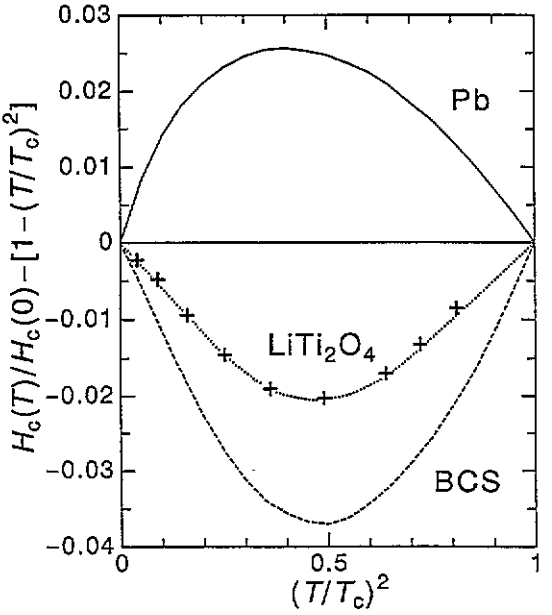

Figure 9. The deviation of the reduced critical field from a parabolic curve as a function of the square of the reduced temperature. The present result for $LiTi_2O_4$ (crosses) is compared with that calculated for a strong-coupling superconductor Pb (full curve) and that obtained from the BCS weak-coupling theory [33] (broken curve).

Finally, the specific heat discontinuity ΔC at T_c is evaluated from the slopes of the critical field deviation at $T = 0$ and T_c [38]. The normalized specific heat discontinuity, $\Delta C/\gamma T_c$ with γ the Sommerfeld constant, is evaluated to be 1.7 for $LiTi_2O_4$. This value agrees fairly well with those observed by the specific heat measurements [5, 6] as listed in table 5. The value of $\Delta C/\gamma T_c$ evaluated for $LiTi_2O_4$ is slightly larger than the value 1.43 predicted in BCS weak-coupling theory [33].

It has been pointed out by Massidda and co-workers [11] that the value of γ observed by the specific heat measurements [5, 6] is somewhat larger than their theoretical value, if only the mass enhancement due to the electron–phonon interaction is considered. Their suggestion is also true for the result in the present paper. By using the expression $\gamma = \frac{1}{3}\pi^2 k_B^2 N(E_F)(1+\lambda)$ with $N(E_F) = 3.0$ states eV^{-1} per formula and $\lambda = 0.657$, γ is estimated to be 11.8 mJ mol^{-1} K^{-2}, while the experimental value is 21.4 mJ mol^{-1} K^{-2} [5, 6]. The difference in γ between the theory and the experiments may be attributed to the mass enhancement due to electron correlation and/or spin fluctuation.

5. Summary

In the present paper, the lattice dynamics of $LiTi_2O_4$ has been studied by taking account of the effect of the electron–phonon interaction derived microscopically on the basis of the realistic electronic band structure. It is found that the phonon frequencies in the range 30–80 meV are renormalized remarkably over a wide region of the Brillouin zone, due to the characteristic dependences of the electron–phonon interaction on wavevectors and vibrational modes.

From the microscopic calculation, it is found that $\alpha^2F(\omega)$ of $LiTi_2O_4$ takes large values in the frequency range 30–80 meV, where phonon frequencies are renormalized remarkably. With the use of $\alpha^2F(\omega)$, λ and $\langle\omega\rangle_{\ln}$ are evaluated to be 0.657 and 28.2 meV, respectively. By solving the Eliashberg equation, T_c and Δ_0 are evaluated to be 10.9 K and 1.79 meV, respectively. The obtained values of $2\Delta_0/k_BT_c = 3.84$ and $\Delta C/\gamma T_c = 1.7$ are slightly larger than the values predicted in the BCS weak-coupling theory, 3.53 and 1.43, respectively. These evaluated values are in good agreement with the observations. The tunneling spectra and the critical field deviation calculated for $LiTi_2O_4$ show some differences from those obtained from the BCS weak-coupling theory. However, the differences are relatively small compared with typical strong-coupling superconductors.

In conclusion, the superconducting properties of $LiTi_2O_4$ can be well interpreted in the framework of the usual phonon-mediated pairing mechanism. Further, it is suggested that $LiTi_2O_4$ is a superconductor that has a pairing interaction of intermediate strength.

Acknowledgments

This work is partly supported by a Grant-in-Aid of Scientific Research on Priority Areas, 'Science of High T_c Superconductivity' by the Ministry of Education, Science and Culture, Japan.

References

[1] Johnston D C 1976 *J. Low Temp. Phys.* **25** 145
[2] van Maaren N H, Schaeffer G M and Lotgering F K 1967 *Phys. Lett.* **25A** 238
[3] Robbins M, Willens R H and Miller R C 1967 *Solid State Commun.* **5** 933
[4] Shelton R N, Johnston D C and Adrian H 1976 *Solid State Commun.* **20** 1077
[5] McCallum R W, Johnston D C, Luengo C A and Maple M B 1976 *J. Low Temp. Phys.* **25** 177
[6] Heintz J M, Drillon M, Kuentzler R, Dossmann Y, Kappler J P, Durmeyer O and Gautier F 1989 *Z. Phys.* B **76** 303
[7] Ng K W, Shelton R N and Wolf E L 1985 *Phys. Lett.* **110A** 423
[8] Ng K W, Khim Z G, Shum D P and Wolf E L 1987 *Surf. Sci.* **181** 37
[9] Ekino T and Akimitsu J 1990 *Physica* B **165–166** 1599
[10] Satpathy S and Martin R M 1987 *Phys. Rev.* B **36** 7269
[11] Massidda S, Yu J and Freeman A J 1988 *Phys. Rev.* B **38** 11352
[12] Gaspari G D and Gyorffy B L 1972 *Phys. Rev. Lett.* **28** 801
[13] McMillan W L 1968 *Phys. Rev.* **167** 331
[14] Eliashberg G M 1960 *Sov. Phys.–JETP* **11** 696; 1961 *Sov. Phys.–JETP* **12** 1000
[15] Shirai M, Suzuki N and Motizuki K 1990 *J. Phys.: Condens. Matter* **2** 3553
[16] Motizuki K, Shirai M and Suzuki N 1991 *Electron–Phonon Interaction in Oxide Superconductors* ed R Baquero (Singapore: World Scientific) p 176
[17] Shirai M, Kinoshita T and Motizuki K 1993 *Int. Conf. on the Physics of Transition Metals* ed P M Oppeneer and J Kübler (Singapore: World Scientific) p 182
[18] Motizuki K and Shirai M 1993 *Physica* B **186–188** 816

[19] Motizuki K and Shirai M *Proc. 2nd CINVESTAV Superconductivity Symp.* at press
[20] Oda T, Shirai M, Suzuki N and Motizuki K 1994 *J. Supercond.* **7** 555
[21] Edwards P P, Egdell R G, Fragala I, Goodenough J B, Harrison M R, Orchard A F and Scott E G 1984 *J. Solid State Chem.* **54** 127
[22] Durmeyer O, Kappler J P, Braurepaire E, Heintz J M and Drillon M 1990 *J. Phys.: Condens. Matter* **2** 6127
[23] Motizuki K and Suzuki N 1986 *Structural Phase Transitions in Layered Transition-Metal Compounds* ed K Motizuki (Dordrecht: Reidel) p 1
[24] Lauwers H A and Herman M A 1980 *J. Phys. Chem. Solids* **41** 223
[25] Himmrich J and Lutz H D 1991 *Solid State Commun.* **79** 447
[26] Gompf F, Renker B and Mutka H 1992 *Physica* B **180–181** 459
[27] Allen P B 1980 *Dynamical Properties of Solids* 3 ed G K Horton and A A Maradudin (Amsterdam: North-Holland) p 95
[28] Allen P B and Mitrović B 1982 *Solid State Phys.* **37** ed H Ehrenreich, F Seitz and D Turnbull (New York: Academic) p 1
[29] Rainer D and Bergmann G 1974 *J. Low Temp. Phys.* **14** 501
[30] Carbotte J P 1990 *Rev. Mod. Phys.* **62** 1027
[31] Bergmann G and Rainer D 1973 *Z. Phys.* **263** 59
[32] Marsiglio F, Schossmann M and Carbotte J P 1988 *Phys. Rev.* B **37** 4965
[33] Bardeen J, Cooper L N and Schrieffer J R 1957 *Phys. Rev.* **108** 1175
[34] Wada Y 1964 *Phys. Rev.* **135** A1481
[35] Bardeen J and Stephan M 1964 *Phys. Rev.* **136** A1485
[36] McMillan W L and Rowell J M 1965 *Phys. Rev. Lett.* **14** 108; 1969 *Superconductivity* ed R D Parks (New York: Marcel Dekker) p 561
[37] Swihart J C, Scalapino D J and Wada Y 1965 *Phys. Rev. Lett.* **14** 106
[38] Scalapino D J 1969 *Superconductivity* ed R D Parks (New York: Marcel Dekker) p 449